

Comparison of sensitivity to color changes in natural and phase-scrambled scenes

Ali Yoonessi* and Frederick A. A. Kingdom

McGill University, Department of Ophthalmology, McGill Vision Research Unit, 687 Pine Avenue West,
Room H4-14, Montréal, Québec H3A 1A1, Canada

*Corresponding author: ali.yoonessi@mcgill.ca

Received August 29, 2007; accepted December 18, 2007;
posted January 8, 2008 (Doc. ID 86875); published February 13, 2008

Traditionally, thresholds for detecting photometric changes have been measured by using stimuli such as disks or gratings and accounted for in terms of relatively low-level mechanisms in the visual pathway. Therefore one might not expect the higher-order structures that characterize natural scenes to influence thresholds for detecting uniform photometric changes. We compared thresholds for detecting uniform photometric changes for natural and phase-scrambled versions of images of natural scenes. The chromaticity and luminance of every pixel was represented as a vector in a modified version of the MacLeod–Boynton color space and was translated, rotated, or compressed within that color space. Thresholds for all types of transformation were significantly lower in the raw compared with phase-scrambled scenes, and we attribute this to the influence of higher-order structure. © 2008 Optical Society of America

OCIS codes: 330.0330, 330.1720.

1. INTRODUCTION

The behavioral study of color vision has traditionally employed simple stimuli such as patches, gratings, and gabors. Only recently has color vision begun to be studied by using images of natural scenes (e.g., [1–3]). Although natural scenes are complex stimuli, and the data obtained from them often difficult to interpret, they nevertheless offer a unique opportunity to examine the ways in which the visual environment most commonly experienced is special for color vision. In this communication, we consider whether the unique structure of natural scenes influences our ability to detect uniform changes to their luminance and chromaticity.

The “structure” of an image generally refers to the spatiotemporal relations between points in the image. Although the unique structure of natural images is partly a consequence of their $1/f$ -shaped Fourier amplitude spectra [3,4], most of the visible structure of natural scenes lies in their phase spectra, as evidenced by the fact that if one swaps the amplitude and the phase spectra of two different images it is the phase spectra that carries the recognizable image structure [5]. Furthermore, the chromatic and luminance layers of a given scene have closely related phase spectra, because chromatic and luminance changes tend to co-occur at most object boundaries [6–11]. Therefore, the method that naturally lends itself to testing whether the particular structure of natural scenes influences the detection of uniform luminance and chromatic changes applied to them is to compare detection performance between raw and phase-scrambled versions of the scenes. But why might this be interesting?

Hubel and Wiesel [12,13] were the first to find neurons in the primary visual cortex of mammals that operated in a quasilinear fashion, which they termed simple cells (linearity implies that one can predict the response of the

neuron to any stimulus once its response to spots or bars projected onto its excitatory and inhibitory receptive field subregions is known). The evidence for quasilinear neurons in the primary visual cortex was complemented by psychophysical studies suggesting that narrowband linear filters mediated the detection of luminance (e.g., [14,15]), and chromatic [16,17] patterns. In addition, evidence suggests that the luminance and chromatic layers of mixed color-luminance patterns are detected independently [16,18–22] and that any influence they have on each other is not dependent on their spatial phase relations [21,23,24]. Therefore under the most simplistic model of image discrimination, in which we assume that the image is transduced by an array of linear filters, discriminability would be proportional to the average (squared) difference in the responses of the array of filters to the discriminand pair. This average difference will be unaffected by the higher-order structure of the stimulus, because stimulus energy is determined by the amplitude, not phase spectrum. Therefore under the simple linear model, we would not expect any difference in the detectability of uniform luminance–chromatic changes applied to raw and phase-scrambled versions of natural scene images.

Mounting evidence, however, suggests that many, if not most, neurons in the visual cortex are not linear. For example, stimuli falling in regions outside the classical receptive fields of many neurons in V1 can dramatically affect their responses provided the neuron is already active [25–34]. Such contextual modulation is believed to be important for figure–ground segregation [35–37] and reflects a general principle that the visual system is organized to code the useful information in the visual environment in an optimally efficient manner [38–45]. The evidence for nonlinear influences from outside the classical receptive

fields of early stage visual neurons might lead us to expect a difference in the detectability of uniform luminance–chromatic changes applied to raw versus phase-scrambled natural scenes. But in which direction?

The above argument for optimality might lead to the prediction that it should be easier to detect uniform luminance–chromatic changes in raw compared with phase-scrambled images of natural scenes. However, other considerations lead to the opposite prediction. One of the important tasks for vision is to determine the lightnesses and colors of objects in spite of changes to the intensive and spectral content of illumination, processes that are termed, respectively, lightness and color constancy [46] (for reviews see [47,48]). Discounting changes in illumination might result in insensitivity to changes in illumination [49,50]. Given that changes in illumination tend to produce spatially uniform changes in chromaticity–luminance, we might therefore expect the visual system to be relatively insensitive to uniform changes in luminance–chromaticity applied to natural scene images. Indeed, it has been suggested that the visual system is relatively insensitive to all types of natural scene transformation that are involved in perceptual invariance, for example, affine geometric transformations such as image scaling, rotation, and translation, in addition to uniform photometric transformations [51]. Since relative insensitivity to uniform photometric transformations might be observed only in images of natural scenes, the above argument leads to the prediction that we will be less sensitive to uniform color–luminance changes applied to raw, compared with phase-scrambled images of natural scenes.

It does not necessarily follow, however, that discounting the illuminant in order to determine object color renders the system insensitive to the illuminant. We are sensitive to nonuniform illumination, such as shadows, shading, and specular reflections, and evidence continues to accrue that we are also sensitive to changes in uniform illumination [52–55], precisely because uniform illumination changes can be useful for helping determine object color [48,49,56,57]. On these grounds we would expect sensitivity to be higher for raw compared with phase-scrambled natural scenes.

In summary, different considerations lead to three different predictions as to the relative sensitivity of observers to uniform color–luminance changes applied to raw and phase-scrambled natural scenes: less sensitive, equally sensitive, and more sensitive.

In order to compare the various types of luminance–chromatic transformation, we have measured thresholds defined in terms of a simple and intuitively appealing metric of image distance: the Euclidean distance, or L_2 norm. If the images are trilayered, RGB colored images, as in Fig. 1, E can be calculated by using the following formula:

$$E = \sqrt{\frac{\sum_{n=1}^N \sum_{i=1}^3 (p_{ni} - q_{ni})^2}{3N}}, \quad (1)$$

where p_{ni} and q_{ni} are the intensities of the corresponding pixels in the two images, with i the image layer ($i=1:3$)

R,G,B), n the pixel (i.e., with a unique x,y coordinate), and N the number of pixels per image. Euclidean distance has the important property that it defines a straightforward measure of the distance between two images and provides the same answer irrespective of the orthonormal basis used to represent the images, e.g., pixels, Fourier, Haar, etc. [58]. Euclidean distance has been previously employed to compare sensitivities to a variety of transformations applied to natural scenes [59]. It is important to state at the outset, however, that we are not arguing that Euclidean distance is the proper perceptual metric. Rather, we argue that E is a relatively neutral metric, providing a useful measure for comparing the relative sensitivities to the different types of color–luminance transformation shown in Fig. 1.

According to the simple linear model described above, threshold E 's would be expected to be the same for raw and phase-scrambled scenes. On the other hand, if we adhere to the idea suggested by Kingdom *et al.* [59], namely, that we are relatively insensitive to those transformations that are involved in perceptual invariance, and add the caveat that the relative insensitivity will be most pronounced in raw scenes, then we would predict higher threshold E 's for the raw compared with phase-scrambled scenes. Finally, on the grounds that the visual system has evolved specialized mechanisms to detect changes in natural scene illumination, then we predict that threshold E 's for uniform color–luminance changes will be lower in raw compared with phase-scrambled images scenes.

In the experiments described below, pixel values were represented as points in a modified version of the Macleod–Boynton color space (as suggested by Ruderman *et al.* [7]), which consists of a luminance and two chromatic axes, known as “red–green” and “blue–yellow.” The transformations applied to the color space were translation, rotation, and compression.

2. METHODS

A. Equipment and Calibration

The scenes were photographed with a Nikon CoolPix-7500 digital camera and displayed on a Sony FD Trinitron 17 in., GDM F-500 using the VSG graphics board (Cambridge Research Systems) housed in an 1800 MHz PC computer. The monitor RGB phosphors were gamma corrected after calibration using an optical photometer (Cambridge Research Systems). The spectral emission functions of the three phosphors were measured by using an Optikon SpectroScan® PR 645 spectrophotometer, with the monitor screen filled with red, green, or blue, in the range 400–700 nm at 10 nm intervals. Monitor resolution was 640×480 with a refresh rate of 100 MHz. Matlab version 7 was used for all image processing tasks.

The cameras were calibrated as follows. Each one of a set of gray Munsell papers was illuminated by an incandescent light with a constant-DC power and photographed. Additionally, the luminance of the light reflected from each paper was measured with a Topcon SR-1 spectroradiometer. The average R, G, and B pixel values were plotted against the corresponding measured luminance and fitted with the following function: $L = a(b^s + 1)$, where L is luminance, s is the pixel level value obtained for each

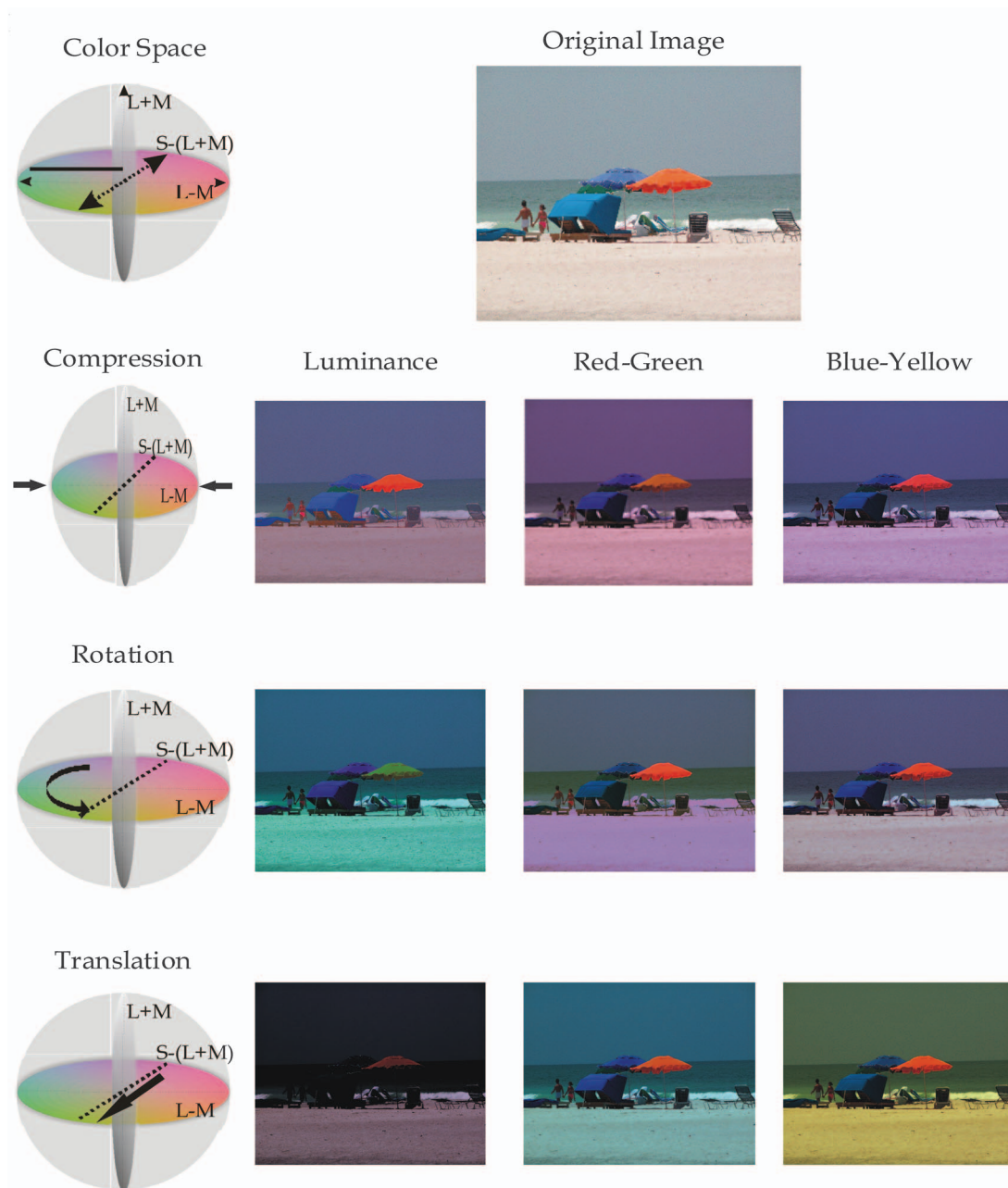


Fig. 1. Different transformations on a sample image.

of the camera sensors (R , G , and B), and b is a constant that determines the slope of the curve. In addition, a white target was photographed through a series of narrowband optical interference filters from 400 to 700 nm at 10 nm intervals. Each R , G , and B value was recorded, gamma corrected, and used to construct a spectral sensitivity function for each sensor, which was then normalized to produce equal responses of to a flat-spectrum light.

B. Images

The linearized camera RGBs were mapped onto linearized monitor RGBs by using a 3×3 linear transformation matrix. The coefficients in the matrix were device specific

and were chosen to produce as faithful a reproduction of the image colors as possible, using a method described in detail elsewhere ([60]).

Fifty everyday scenes, representing a range of natural environments (forests, mountains, flowers, and fruits) and urban scenes (buildings, traffic signs, man-made objects), photographed under a variety of different illumination conditions (sunny and cloudy) and at a variety of distances (0.5–1000 m), were taken from the McGill Calibrated Color Image database [59]. The images were photographed by the camera (see above) and stored as uncompressed Tagged Image File Format (TIFF) files with resolution 1920×2560 pixels and color depth of 24 bits (256 levels for each R , G , and B image). The camera's

smallest aperture setting ($f7.4$) was chosen to capture the images with minimum within-image differences in focus. Then, the images were resized to 147×147 pixels wide by using a nearest-neighbor interpolation algorithm and then converted to bitmap file format with 24 bit depth. Each image subtended 9×9 cm (5.7° of visual angle) on the monitor at the viewing distance of 90 cm.

C. Stimulus Procedures

Phase-scrambled images. Phase randomization was applied to the phase spectra of the images using a discrete Fourier transform. The phase and amplitude spectra were calculated using the following formulas:

$$\text{Amplitude} = \sqrt{[F_r(\omega_x, \omega_y)^2 + F_i(\omega_x, \omega_y)^2]},$$

$$\text{Phase} = \arctan \left[\frac{F_i(\omega_x, \omega_y)}{F_r(\omega_x, \omega_y)} \right],$$

where ω_x and ω_y are frequency variables and F_r and F_i are

the real and imaginary parts of each Fourier frequency component. A random number between $-\pi$ and $+\pi$ was assigned to each Fourier component phase in all three image layers. An inverse Fourier transform then returned the phase-scrambled image (Fig. 2).

Conversion of stimuli from RGB to LMS color space. Using the spectral sensitivities of the camera sensors and the sensitivities of the L (long-), M (middle-) and S (short-wavelength-sensitive) cones provided by Smith and Pokorny [61], a conventional 3×3 linear matrix was used to convert the RGB camera values to LMS cone excitations [59].

Color space and post-receptoral layers. A modified version of the Ruderman color space was used to model the three postreceptoral layer images [7]. Cone contrasts for each pixel were defined as

$$\mathcal{L}_C = \log L - \overline{\log L}, \quad \mathcal{M}_C = \log M - \overline{\log M},$$

$$\mathcal{S}_C = \log S - \overline{\log S}, \tag{2}$$

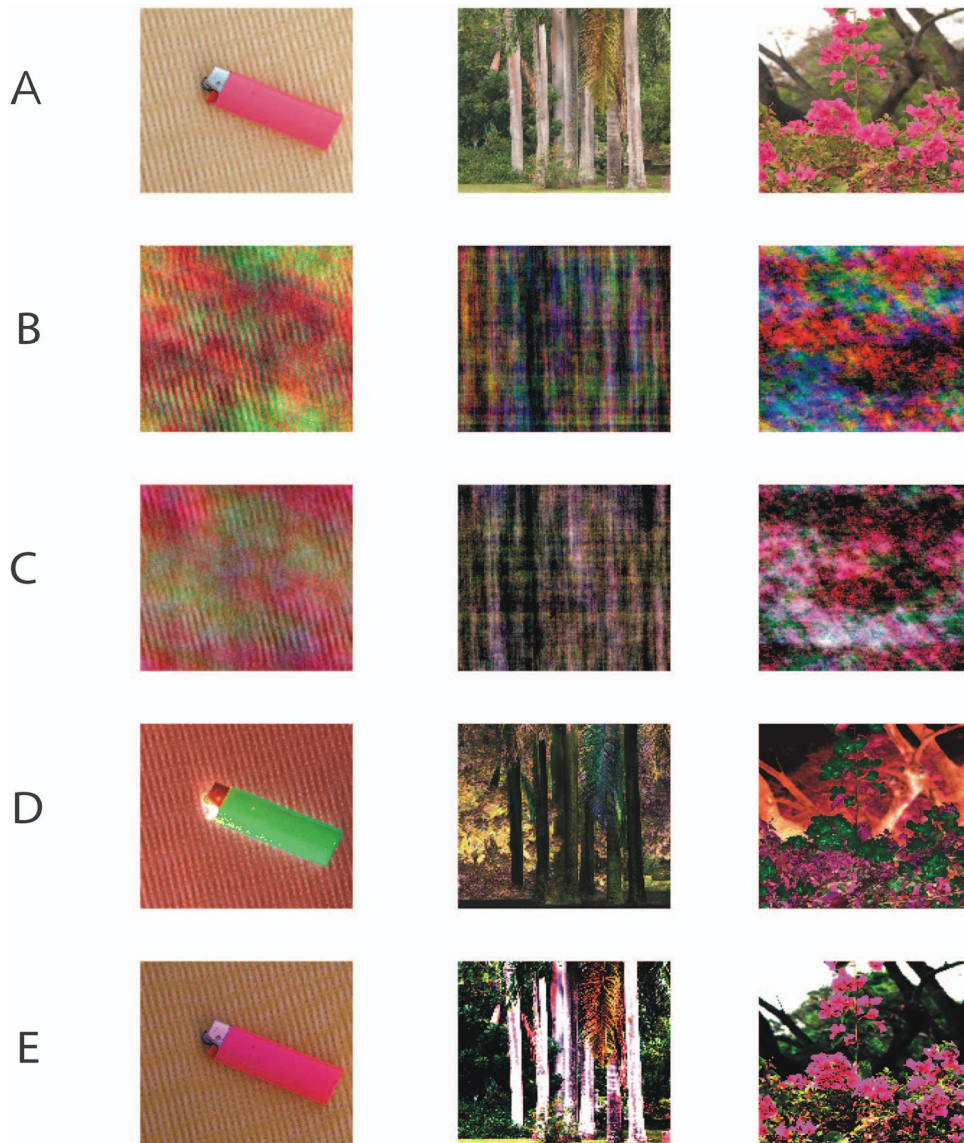


Fig. 2. A, Three sample raw images; B, phase scrambled; C, phase-aligned phase-scrambled; D, reverse; E, raw color transfer.

where $\log L$, $\log M$, and $\log S$ are log pixel cone excitations and $\overline{\log L}$, $\overline{\log M}$ and $\overline{\log S}$ log pixel cone excitations averaged across the image. The postreceptoral responses to each pixel were defined as

$$\hat{l} = (r\hat{L}_C + \hat{M}_C), \quad \hat{\alpha} = (\hat{L}_C + \hat{M}_C - 2\hat{S}_C), \quad \hat{\beta} = (\hat{L}_C - \hat{M}_C), \quad (3)$$

where $\hat{l}, \hat{\alpha}, \hat{\beta}$ are the luminance, blue–yellow, and red–green axes, respectively. r is a parameter that determines the relative L and $\log L$ cone contrast inputs to the luminance mechanism and varies between observers. We determined r as described below.

Image transformations. We applied three transformations to the color space: compression, translation, and rotation. All transformations were affine; that is, all points lying on a line remained on the line after the transformation, and the ratios of distances between points remained the same [62]. Six levels of each transformation, i.e., six levels of E , were employed, and these were determined through pilot experiments. The minimum E was chosen to produce performance just above chance level, and the maximum E was chosen to produce performance above 90%. The six values of E were logarithmically spaced.

D. Psychophysical Procedures

Scaling of axes. To compare transformations across different axes of color space, the axes need to be equated, and for this study we equated them in terms of perceived contrast. Subjects adjusted the contrast of the luminance and red–green layers of five randomly selected images to match the apparent contrast of the blue–yellow layers (the blue–yellow layers had the lowest perceived contrast, so these were chosen as the baseline). The average scaling factors that were found to equate the three layers for perceived contrast were then applied to all images for each subject separately.

Isoluminant setting. Isoluminance was determined by using the method of minimum distinct border [63]. Subjects changed the ratio of L to M in the red–green layers of five randomly selected natural images until the image appeared to have least sharp borders and appeared shimmering. This ratio is the parameter r in the equation above.

Forced-choice design. On each trial, four images were shown to the subject. Each set of four consisted of three original and one transformed image. The four images were presented in two successive pairs in a conventional two-interval-forced-choice procedure. Each pair of images was presented side-by-side on the screen with a center-to-center separation of 13.5 cm, or 8.6°. The transformed image was randomly presented in either the first pair or the second pair, and either on the left or the right side of the pair. The interstimulus interval was 200 ms, and each image was displayed for 250 ms. The subject's task was to identify the interval in which the pair appeared different. A tone provided feedback for an incorrect response. For each session, the transformation and layer type was fixed, while the sequence of images was selected randomly. There were 150 trials per session, and two sessions per condition, giving a total of 300 trials per condition. All three subjects had normal or corrected-to-normal vision, and color vision was tested by using the Ishihara plates.

Analysis. On every trial the Euclidean distance E of the transformed image was recorded along with the subject's response (correct or incorrect). Although there were six discrete levels for each transformation, the computed values of E for each level of a given transformation varied according to image. In order to fit psychometric functions to the data, the E 's were divided into six bins for each transformation. The first bin was set to have a minimum of zero, while the last, sixth bin was set to have a maximum equal to the maximum E found for that transformation. The first bin divider was determined iteratively to be that value of E that minimized the between-bin variance in the number of trials when the remaining bin dividers were logarithmically spaced. This method ensured that the trials were distributed as evenly as possible between bins while obeying the constraint that all bins except the first bin were logarithmically spaced (E 's in the first bin began at zero). After the E 's were binned, the mean $\log(E)$, correct proportion, and number of trials were calculated for each bin.

Psychometric functions were fitted by using psignifit version 2.5.6, which uses the maximum-likelihood method described by Wichmann and Hill [64].

3. RESULTS

Example psychometric functions for translation of the blue–yellow layer, for both raw and phase-scrambled scenes, are shown in Fig. 3. Each plot gives the overall proportion correct trials as a function of $\log(E)$. The threshold was calculated at the 75% correct level (see Section 2).

Thresholds for all four types of transformation and for both raw and phase-scrambled images are shown in Fig. 4. As can be seen, thresholds for the phase-scrambled images are systematically higher than for the raw images. Averaged across transformation and subjects, threshold $\log(E)$ values are 1.1 for the raw and 1.17 for the phase-scrambled images, a 17% difference. A four-way within-subject analysis of variance with factors type of image (raw versus phase-scrambled), layer (luminance, red–green, blue–yellow), transformation (translation, positive and negative; rotation, clockwise and counterclockwise; and compression), and subjects was conducted. The difference between raw and phase-scrambled scenes was significant at the $p=0.05$ level ($F=19.69$, $df=1$, $p=0.047$). Although the transformations involving the luminance and blue–yellow axes produced on average higher thresholds than those involving the red–green layer, there was no significant effect of layer (Fig. 4).

A. Changes to the Color Histogram

Phase-aligned phase-scrambling method. In this experiment we ask whether the higher sensitivity that we found for uniform color–luminance changes in raw compared with phase-scrambled images of natural scenes is due to the changes in the color histogram that occur when images are phase scrambled. As can be seen from Fig. 1, our method of phase scrambling introduces new colors. In this experiment, as suggested by Prins [65], the same phase shift is applied to each image layer, thus preserving the phase relations among layers and as a consequence pre-

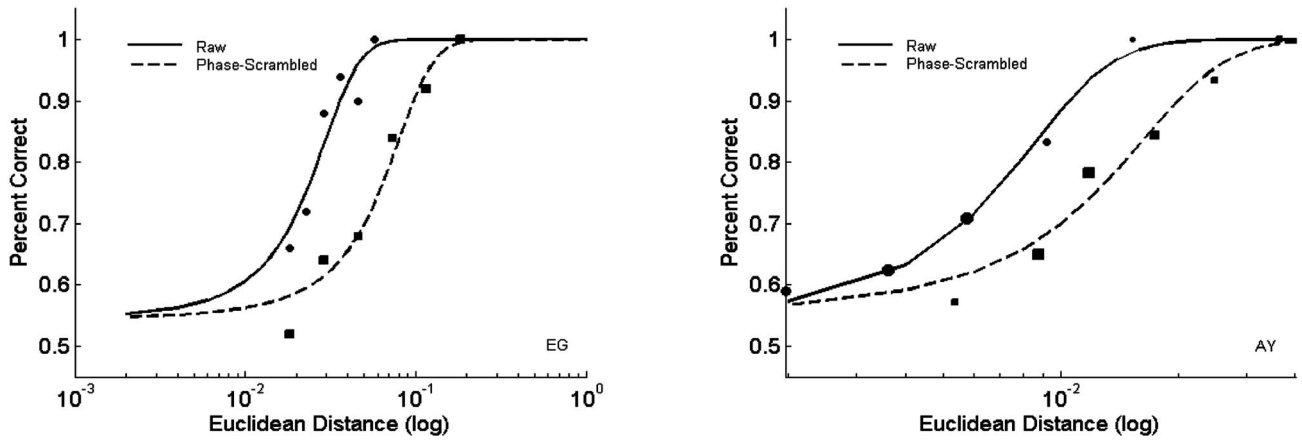


Fig. 3. Comparison of percentage correct in raw and phase-scrambled scenes in two transformations, translation in blue–yellow layer on left, and compression of luminance layer on right.

servicing the color histogram more faithfully, as can be seen from Fig. 1. We measured the thresholds for two transformations, translation and rotation, and two layers, luminance and red–green, in two subjects. The results are shown in Fig. 5. A paired one-tailed *t* test shows that the difference in thresholds is again significant [$t(7)=2.45, p=0.042$]. This suggests that changes to the color histogram introduced by phase scrambling is not the

main reason why sensitivity to uniform colors–luminance is higher in raw compared with phase-scrambled natural scenes.

Color transfer method. The color histogram resulting from the above method of phase scrambling is still slightly different from that of the original scene. Therefore we tested another method to equalize the histogram, suggested by Reinhard *et al.* [66]. In this method the color

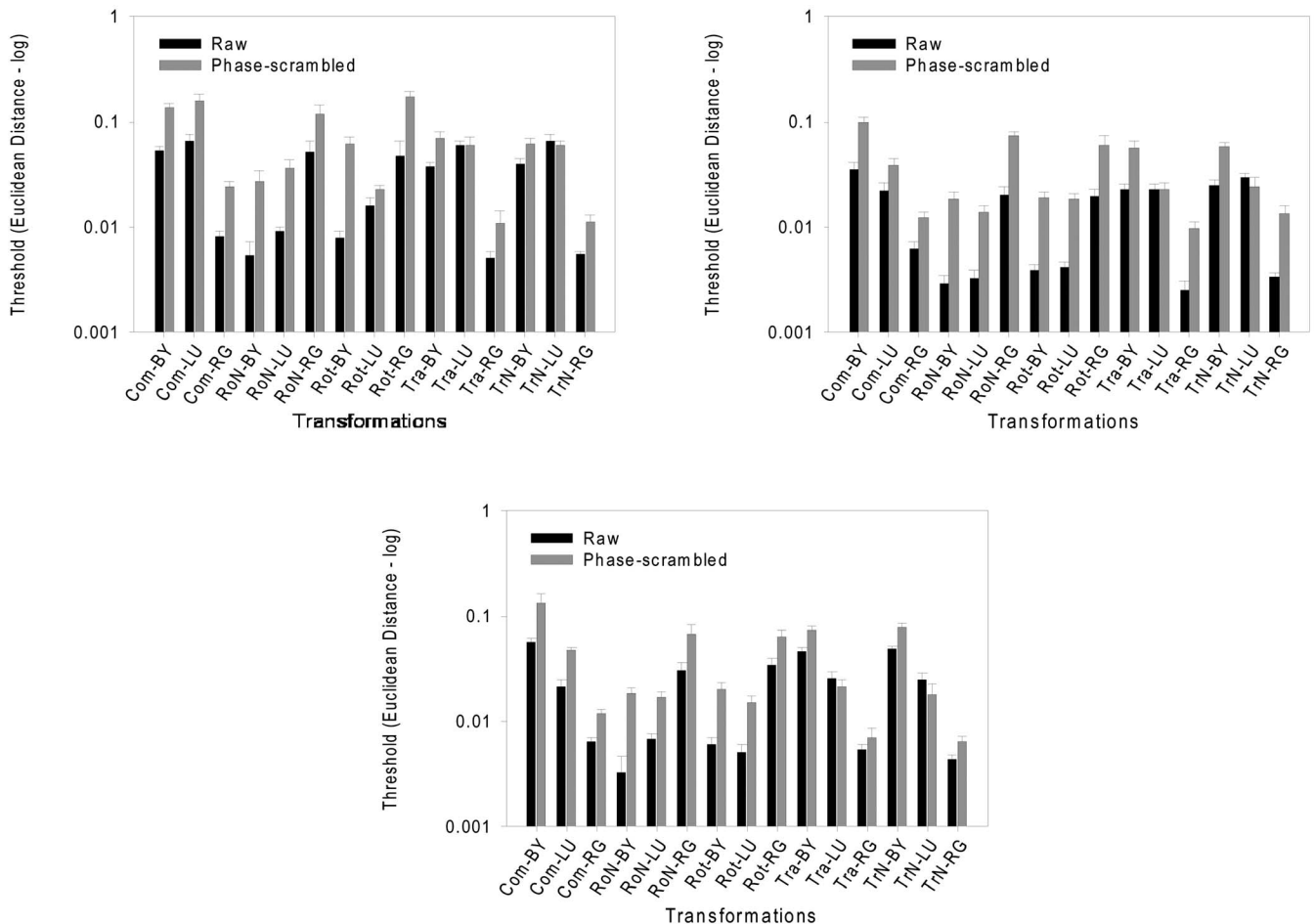


Fig. 4. Thresholds for different types of transformation–layers in three subjects (Com, compression; RoN, rotation negative; Rot, rotation; Tra, translation; TrN, translation negative).

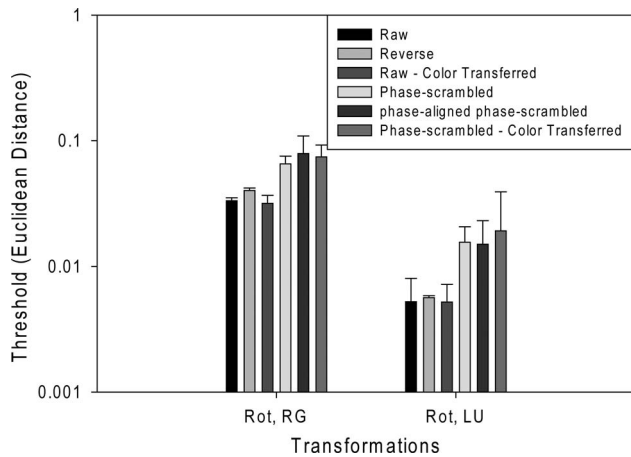


Fig. 5. Comparison of thresholds for all six types of images in one subject.

content of the raw images was transferred to the phase-scrambled images and vice versa, as follows. First, for each image, we computed the standard deviation (SD) of the pixel histogram of each layer in the Ruderman color space. Then, we computed the ratio of SDs of the source (raw or phase scrambled) to the target (phase scrambled or raw) for each layer. Finally, each pixel in each layer of the Ruderman color space was multiplied by the SD ratio, and the resulting new values converted back to the RGB color space (Fig. 1). The new target images had colors similar to the source images. Thresholds were measured for both the new raw and new phase-scrambled images for translation and rotation in the luminance and red-green layers. The results are shown in Fig. 5. The differences between the raw and phase-scrambled images in both original and color-transfer manipulations were again significant [original $t(7)=2.88$, $p=0.02$; color transfer, $t(7)=2.85$, $p=0.02$]. A paired two-tailed t test on the difference of the phase-scrambled and the color-transfer version of the same phase-scrambled image did not show any significant difference [$t(7)=0.76$, $p=0.47$]; neither did comparison of original and new raw images [$t(7)=0.656$, $p=0.53$].

B. Structure versus Familiarity

In this experiment we ask whether the higher sensitivity to uniform color-luminance in raw compared with phase-scrambled images of natural scenes is due to the presence of higher-order structure or due to the presence of familiar colors and luminances. To test between these two possibilities, we reversed the colors and luminances of the images in the Ruderman color space (Fig. 2). Thus a pixel whose color was at point \hat{l} , $\hat{\alpha}$, $\hat{\beta}$ in the color space would be reallocated the color $-\hat{l}$, $-\hat{\alpha}$, $-\hat{\beta}$. The resulting images had the same structure as natural scenes, but with opposite colors and luminances. As with the previous experiment, thresholds were measured for four transformation-layer combinations: translation and rotation, for the luminance and red-green layers. The color-reversed thresholds in general lay between the raw and the phase-scrambled thresholds. A student's t test revealed a significant difference between the color-reversed and phase-scrambled thresholds (mean reverse 0.06, mean phase 0.11, t (re-

verse versus phase)=2.83, p (reverse versus phase)=0.01), but not between the raw and color-reversed thresholds (mean real 0.05, mean reverse 0.06, t (natural versus reverse)=0.351, p (natural versus reverse)=0.729). These results suggest that higher-order structure rather than color-luminance familiarity is the main reason why sensitivity to uniform colors-luminance is higher in raw compared with phase-scrambled natural scenes (Fig. 5).

4. DISCUSSION

Sensitivity for detecting uniform color-luminance changes was higher for raw compared with phase-scrambled images of natural scenes. As argued in Section 1, this result is unexpected from the point of view of linear systems analysis, which assumes that simple color-luminance changes are detected by arrays of linear filters in the early visual cortex. Familiarity of object colors and luminances does not appear to be the main factor responsible for the superior sensitivity in raw versus phase-scrambled images, nor do the changes to the color histogram that occur when a raw scene is phase scrambled. Rather, the results support the idea that when processing uniform photometric changes, the visual system is optimized for the particular structural characteristics of natural scenes.

What is it about the higher-order structure that produces higher sensitivity to uniform photometric transformations? Raw images of natural scenes contain regions of uniform color and luminance not found in their phase-scrambled counterparts, and perhaps it is this that underlies the higher sensitivity. The size of uniform areas is inversely related to the degree of image randomness, and one measure of image randomness is entropy—the higher the entropy the greater the randomness [40,67,68]. For our images we used the Matlab function of entropy, defined as $-\sum(p \cdot \log(p))$, where p is the histogram counts of pixels of the image. Using this measure, entropy for the luminance layer was greater for phase-scrambled compared with raw scenes (4.82 and 3.75, respectively). To test the idea that entropy might be the correlate of performance we correlated the entropy of each image with its associated number of correct responses. A negative correlation between image entropy and number correct might be expected. The strongest negative correlations were found for the luminance transformations, for both raw ($R=-0.47$) and phase-scrambled ($R=-0.45$) scenes. For the blue-yellow transformations, a negative correlation was found for the raw ($R=-0.42$) but not phase-scrambled ($R=0.47$) scenes, and for the red-green layers a negative correlation was found for phase-scrambled ($R=-0.32$) but not raw ($R=0.17$) scenes. However, the conventional measure of entropy is probably not the best measure of patchiness, since it does not explicitly take into account the relative positions of pixel values (if the pixels of an image are randomly re-allocated, the measure entropy does not change). Thus while entropy appears to capture the difference in performance between raw and phase-scrambled scenes, it does not consistently predict performance on an image-by-image basis for the various classes of image transformation.

Kingdom *et al.* [51] have shown that transformations applied to natural scenes that are involved in perceptual invariance are less easily detected than other types of transformation. They found that affine geometric transformations, such as image rotation, scaling, and translation, applied to images of natural scenes were an order of magnitude more difficult to detect than the addition of random noise. Thresholds for detecting uniform photometric changes, such as brightening or reducing contrast, which are similar to the uniform color–luminance changes employed here, fell in between the affine-geometric and added-noise thresholds. If the relative insensitivity to transformations involved in perceptual invariance manifest itself only in the context of real scenes, we would expect sensitivity to the phase-scrambled scenes to be higher, not lower than the raw images. The fact that the opposite was found suggests that perceptual invariance is dependent on the type of transformation applied to the image, not on the type of image. If so, we would predict a similar ordering of thresholds (geometric > photometric > added noise) applied to phase-scrambled images of natural scenes, even though overall thresholds would be higher than for raw scenes. We are currently testing this prediction.

5. CONCLUSION

The higher-order structural properties of natural scenes influences our ability to detect uniform changes in their color and luminance composition. The patchiness of natural scenes is the most likely reason why thresholds for detecting uniform color–luminance changes is lower for natural compared with phase-scrambled scenes.

ACKNOWLEDGMENTS

We thank Adriana Olmos for calibrating the camera and providing the images of natural scenes, and David Field and Aaron Johnson for their helpful suggestions. We also thank two reviewers for their useful comments. This study was supported by Canadian Institute of Health Research Grant 11554 to F.A.A. Kingdom.

REFERENCES

1. M. A. Webster and J. D. Mollon, "Adaptation and the color statistics of natural images," *Vision Res.* **37**, 3283–3298 (1997).
2. D. H. Brainard, M. D. Rutherford, and J. M. Kraft, "Color constancy compared: experiments with real images and color monitors," *Invest. Ophthalmol. Visual Sci.* **38**, 2206–2206 (1997).
3. C. A. Párraga, T. Troscianko, and D. J. Tolhurst, "Spatiochromatic properties of natural images and human vision," *Curr. Biol.* **12**, 483–487 (2002).
4. D. J. Tolhurst, Y. Tadmor, and T. Chao, "Amplitude spectra of natural images," *Ophthalmic Physiol. Opt.* **12**, 229–232 (1992).
5. L. N. Pirotrowski and F. W. Campbell, "A demonstration of the visual importance and flexibility of spatial-frequency amplitude and phase," *Perception* **11**, 337–346 (1982).
6. J. M. Rubin and W. A. Richards, "Color vision and image intensities: when are changes material?" *Biol. Cybern.* **45**, 215–226 (1982).
7. D. L. Ruderman, T. W. Cronin, and C. C. Chiao, "Statistics of cone responses to natural images: implications for visual coding," *J. Opt. Soc. Am. A* **15**, 2036–2045 (1998).
8. I. Fine, A. R. Wade, A. A. Brewer, M. G. May, D. F. Goodman, G. M. Boynton, B. A. Wandell, and D. I. A. MacLeod, "Long-term deprivation affects visual perception and cortex," *Nat. Neurosci.* **6**, 915–916 (2003).
9. M. F. Tappen, W. T. Freeman, and E. H. Adelson, "Recovering intrinsic images from a single image," *Adv. Neural Inf. Process. Syst.* **15**, 1459–1472 (2002).
10. A. Olmos and A. A. Frederick, "A biologically inspired algorithm for the recovery of shading and reflectance images," *Perception* **33**, 1463–1473 (2004).
11. A. P. Johnson, F. Kingdom, and C. J. Baker, "Spatiochromatic statistics of natural scenes: first- and second-order information and their correlational structure," *J. Opt. Soc. Am. A* **22**, 2050–2059 (2005).
12. D. H. Hubel and T. N. Wiesel, "Receptive fields, binocular interaction and functional architecture in the cat's visual cortex," *J. Physiol. (London)* **160**, 106–154 (1962).
13. D. H. Hubel and T. N. Wiesel, "Receptive fields and functional architecture of monkey striate cortex," *J. Physiol. (London)* **195**, 215–243 (1968).
14. C. Blakemore and F. W. Campbell, "On the existence of neurones in the human visual system selectively sensitive to the orientation and size of retinal images," *J. Physiol. (London)* **203**, 237–260 (1969).
15. D. Ferster, "Spatially opponent excitation and inhibition in simple cells of the cat visual cortex," *J. Neurosci.* **8**, 1172–1180 (1988).
16. A. Bradley, E. Switkes, and K. De Valois, "Orientation and spatial frequency selectivity of adaptation to color and luminance gratings," *Vision Res.* **28**, 841–856 (1988).
17. M. J. Sankeralli and K. T. Mullen, "Postreceptoral chromatic detection mechanisms revealed by noise masking in three-dimensional cone contrast space," *J. Opt. Soc. Am. A* **14**, 2633–2646 (1997).
18. B. A. Wandell, "Color measurement and discrimination," *J. Opt. Soc. Am. A* **2**, 62–71 (1985).
19. J. Krauskopf, Q. Zaidi, and M. B. Mandler, "Mechanisms of simultaneous color induction," *J. Opt. Soc. Am. A* **3**, 1752–1757 (1986).
20. G. R. Cole, T. Hine, and W. McIlhagga, "Detection mechanisms in L-, M-, and S-cone contrast space," *J. Opt. Soc. Am. A* **10**, 38–51 (1993).
21. K. T. Mullen and M. A. Losada, "Evidence for separate pathways for color and luminance detection mechanisms," *J. Opt. Soc. Am. A* **11**, 3136–3151 (1994).
22. K. T. Mullen and M. J. Sankeralli, "Evidence for the stochastic independence of the blue–yellow, red–green and luminance detection mechanisms revealed by subthreshold summation," *Vision Res.* **39**, 733–745 (1999).
23. K. K. De Valois and E. Switkes, "Simultaneous masking interactions between chromatic and luminance gratings," *J. Opt. Soc. Am.* **73**, 11–18 (1983).
24. E. Switkes, A. Bradley, and K. K. De Valois, "Contrast dependence and mechanisms of masking interactions among chromatic and luminance gratings," *J. Opt. Soc. Am. A* **5**, 1149–1162 (1988).
25. C. Blakemore and E. A. Tobin, "Lateral inhibition between orientation detectors in the cat's visual cortex," *Exp. Brain Res.* **15**, 439–440 (1972).
26. J. I. Nelson and B. J. Frost, "Orientation-selective inhibition from beyond the classic visual receptive field," *Brain Res.* **139**, 359–365 (1978).
27. J. J. Knierim and D. C. van Essen, "Neuronal responses to static texture patterns in area V1 of the alert macaque monkey," *J. Neurophysiol.* **67**, 961–980 (1992).
28. A. M. Sillito, K. L. Grieve, H. E. Jones, J. Cudeiro, and J. Davls, "Visual cortical mechanisms detecting focal orientation discontinuities," *Nature* **378**, 492–496 (1995).
29. J. R. Cavanaugh, W. Bair, and J. A. Movshon, "Nature and interaction of signals from the receptive field center and surround in macaque V1 neurons," *J. Neurophysiol.* **88**, 2530–2546 (2002).
30. J. B. Levitt and J. S. Lund, "Contrast dependence of contextual effects in primate visual cortex," *Nature* **387**, 73–76 (1997).

31. H. C. Nothdurft, J. L. Gallant, and D. C. Van Essen, "Response modulation by texture surround in primate area V1: correlates of 'popout' under anesthesia," *Visual Neurosci.* **16**, 15–34 (1999).
32. H. E. Jones, K. L. Grieve, W. Wang, and A. M. Sillito, "Surround suppression in primate V1," *J. Neurophysiol.* **86**, 2011–2028 (2001).
33. H. Yao and C. Y. Li, "Clustered organization of neurons with similar extra-receptive field properties in the primary visual cortex," *Neuron* **35**, 547–553 (2002).
34. D. Smyth, B. Willmore, G. E. Baker, I. D. Thompson, and D. J. Tolhurst, "The receptive-field organization of simple cells in primary visual cortex of ferrets under natural scene stimulation," *J. Neurosci.* **23**, 4746–4759 (2003).
35. K. Zipser, V. A. F. Lamme, and P. H. Schiller, "Contextual modulation in primary visual cortex," *J. Neurosci.* **16**, 7376–7389 (1996).
36. N. Petkov and M. A. Westenberg, "Suppression of contour perception by band-limited noise and its relation to nonclassical receptive field inhibition," *Biol. Cybern.* **88**, 236–246 (2003).
37. C. Grigorescu, N. Petkov, and M. A. Westenberg, "Contour and boundary detection improved by surround suppression of texture edges," *Image Vis. Comput.* **22**, 609–622 (2004).
38. H. B. Barlow, "Single units and sensation: a neuron doctrine for perceptual psychology," *Perception* **1**, 371–394 (1972).
39. H. Barlow, "Redundancy reduction revisited," *Network Comput. Neural Syst.* **12**, 241–253 (2001).
40. D. J. Field, "Relations between the statistics of natural images and the response properties of cortical cells," *J. Opt. Soc. Am. A* **4**, 2379–2394 (1987).
41. D. J. Field, "What is the goal of sensory coding?" *Neural Comput.* **6**, 559–601 (1994).
42. B. A. Olshausen and D. J. Field, "Sparse coding with an overcomplete basis set: a strategy employed by V1?" *Vision Res.* **37**, 3311–3325 (1997).
43. B. A. Olshausen and D. J. Field, "Sparse coding of sensory inputs," *Curr. Opin. Neurobiol.* **14**, 481–487 (2004).
44. M. G. A. Thomson, "High-order structure in natural scenes," *J. Opt. Soc. Am. A* **16**, 1549–1553 (1999).
45. M. G. A. Thomson, "Beats, kurtosis and visual coding," *Network Comput. Neural Syst.* **12**, 271–287 (2001).
46. H. von Helmholtz, *Handbuch der Physiologischen Optik* (Leopold Voss, 1867).
47. D. H. Foster, "Does colour constancy exist," *Trends Cogn. Sci.* **7**, 439–443 (2003).
48. H. E. Smithson, "Sensory, computational and cognitive components of human colour constancy," *Philos. Trans. R. Soc. London, Ser. B* **360**, 1329–1346 (2005).
49. Q. Zaidi, "Color constancy in a rough world," *Color Res. Appl.* **26**, S192–S200 (2001).
50. J. Schubert and A. L. Gilchrist, "Relative luminance is not derived from absolute luminance," *Invest. Ophthalmol. Visual Sci. Abstract Book* 2826-3, 1258 (1992).
51. F. A. A. Kingdom, D. J. Field, and A. Olmos, "Does spatial invariance result from insensitivity to change?" *J. Vision* **7**, 1–13 (2007).
52. M. Bhalla and D. R. Proffitt, "Visual-motor recalibration in geographical slant perception," *J. Exp. Psychol. Hum. Percept. Perform.* **25**, 1076–1096 (1999).
53. A. Gilchrist, C. Kossyfidis, F. Bonato, T. Agostini, J. Cataliotti, X. Li, B. Spehar, V. Annan, and E. Economou, "An anchoring theory of lightness perception," *Psychol. Rev.* **106**, 795–834 (1999).
54. M. D. Rutherford and D. H. Brainard, "Lightness constancy: A direct test of the illumination-estimation hypothesis," *Psychol. Sci.* **13**, 142–149 (2002).
55. K. Amano, D. H. Foster, and S. M. C. Nascimento, "Color constancy in natural scenes with and without an explicit illuminant cue," *Visual Neurosci.* **23**, 351–356 (2006).
56. J. Golz and D. I. A. MacLeod, "Influence of scene statistics on colour constancy," *Nature* **415**, 637–640 (2002).
57. L. T. Maloney, "Illuminant estimation as cue combination," *J. Vision* **2**, 493–504 (2002).
58. R. A. Horn and C. R. Johnson, *Matrix Analysis* (Cambridge U. Press, 1985).
59. F. A. A. Kingdom, D. J. Field, and A. Olmos, "Does spatial invariance result from insensitivity to change," *J. Vision* **7**, 1–13 (2004).
60. A. Yoonessi and F. A. A. Kingdom, "Faithful reproduction of colours on a CRT monitor," *Color Res. Appl.* **32**, 388–393 (2007).
61. V. C. Smith and J. Pokorny, "Spectral sensitivity of the foveal cone photopigments between 400 and 500 nm," *Vision Res.* **15**, 161–171 (1975).
62. E. W. Weisstein, *MathWorld—A Wolfram Web Resource*, (CRC Press, 2004).
63. R. M. Boynton, "Implications of the minimally distinct border," *J. Opt. Soc. Am.* **63**, 1037–1043 (1973).
64. F. A. Wichmann and N. J. Hill, "The psychometric function: I. Fitting, sampling, and goodness of fit," *Percept. Psychophys.* **63**, 1293–1313 (2001).
65. N. Prins, Department of Psychology, University of Mississippi, University, Miss. 38677 (personal communication, 2007).
66. E. Reinhard, M. Adhikhmin, B. Gooch, and P. Shirley, "Color transfer between images," *IEEE Comput. Graphics Appl.* **21**, 34–41 (2001).
67. B. A. Olshausen and D. J. Field, "Sparse coding with an overcomplete basis set: a strategy employed by V1," *Vision Res.* **37**, 3311–3325 (1997).
68. E. P. Simoncelli, "Statistical models for images: compression, restoration and synthesis," in *31st Asilomar Conference on Signals, Systems, and Computers* (IEEE, 1997), pp. 673–678.